Article:
Wu, G orcid.org/0000-0003-0795-8898, Li, Y, Brittain, R et al. (2 more authors) (2022) Understanding of fracture conditions and material response in a model TiN film/stainless steel substrate system – A cross-sectional scratch test study. Surface and Coatings Technology, 442. 128340. ISSN 0257-8972

https://doi.org/10.1016/j.surfcoat.2022.128340

Understanding of fracture conditions and material response in a model TiN film/stainless steel substrate system – A cross-sectional scratch test study

Guizhi Wu[a,b,*], Yongjun Li[b], Rob Brittain[a], Zhibin Lu[b], Liuquan Yang[a,*]

a School of Mechanical Engineering, University of Leeds, Leeds, LS2 9JT, United Kingdom

b State Key Laboratory of Solid Lubrication, Lanzhou Institute of Chemical Physics, Chinese Academy of Sciences, Lanzhou, 730000, China

Corresponding Author.

Email Address: G.Z.Wu@leeds.ac.uk (G.Z. Wu); L.Q.Yang@leeds.ac.uk (L.Q. Yang)

Abstract:

The assessment of adhesion property of thin films by scratch test method is still a big challenge, relying on understanding accurately the material response and failure modes during scratch. In this study, a model TiN film on stainless steel substrate was studied by carrying out scratch tests. The entire scratch tracks were observed cross-sectionally and by superficial analysis to characterize its adhesion properties, scratch failures, and material response. Other than cracks and ploughing wear, a series of microscopic deformations and fracture mechanisms were observed and formed the overall material response of the model TiN/substrate system. These responses included substrate plastic deformation, synergistic bulge deformation at the scratch track edge, pile-up in front of the stylus, and fragmentation of TiN film. The spallation failure at the edge of track, where the first spallation was generally assigned as critical load (Lc) Lc2 and features an adhesive failure, was found to be cohesive failure. Furthermore, the Lc3 site corresponded to cohesive failure in the substrate rather than the adhesive failure of the film peeling off completely. Therefore, the results of this study indicate more care should be paid in terms of using Lc to interpret the adhesion properties of other film/substrate systems. The adhesion of film should be evaluated by considering the whole film/substrate system, not solely superficial analysis of the film surface.

Keywords: Scratch test; TiN film, Failure modes; Critical loads; Adhesive and cohesive

Graphical Abstract:

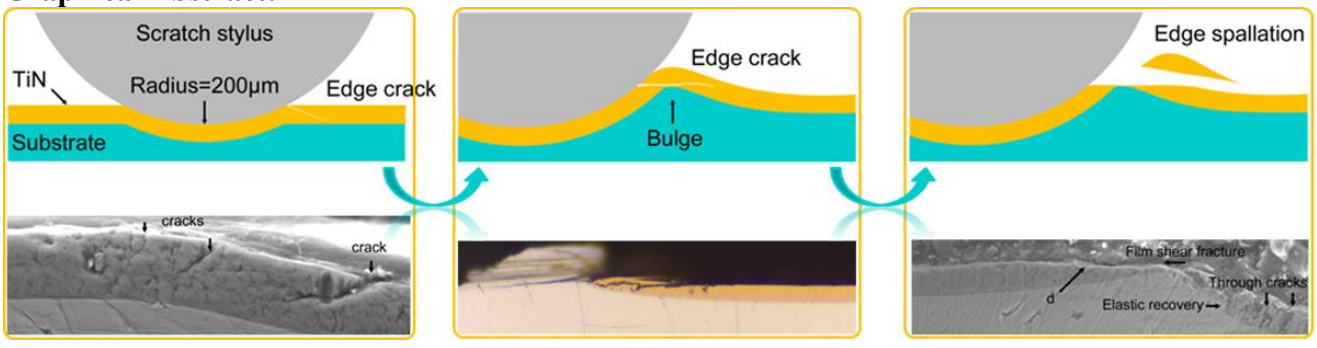

1. Introduction

Scratch testing is a commonly used method to assess the coating adhesion strength both in academic research and industrial fields[1, 2], due to its practical setups and quasi-quantitative measurements[3]. The related mechanism is also deemed as a basic theory in tribology, for its importance in studying tribological contact mechanisms. In comparison with other coating adhesion evaluation methods, it is used particularly in cases where the coating/substrate adhesion are strong.

The critical load (Lc) of film adhesion strength is defined as the load at which the coating is generally believed to indicate different types of failures from the substrate[4] to evaluate film adhesion strength in scratch testing as early as 1980s. Although the definition of Lc is understandable, it is difficult to locate where the first coating detachment failure occurs. Furthermore, the Lc values cannot be confirmed solely by using the first sudden rise of the acoustic signal in many scratch tests[1]. It is known that the contact mechanism and the failure mechanism during the scratch process are too complex that simple acoustic signal is insufficient to evaluate the film strength. Due to the way the data acquisition was designed in the current standardized equipment, Lc values were determined by acoustic emission (AE) signal. The links between the Lc values to the coating performance have been weakened through the development of coating technology, making previous test criteria insufficient. It was found that initial AE peak represents cohesive-related coating internal crack generation and propagation more than that of adhesive-related coating peeling, since the AE signal would occur at crack initiation, growth and closure, etc[1]. Meanwhile, only a few possible failure modes are adhesion related, and the mechanical performances of coatings vary with their compositions, structures and thicknesses. Bromark et al.[5] argued that a thorough post-test scratch inspection was important in evaluating coating adhesion strength. As a result, researchers generally combine the AE signal and post-test analysis of the scratch track using optical microscope or electron microscope observations to evaluate the film adhesion strength[1]. However, the failure modes are still unclear from the microscopic study so far correlating to the AE signals.

It is found that soft and hard coatings along with the substrate hardness or substrate surface topography will influence the contact mechanisms. Thus it would induce different failure modes during a scratch test[5], leading to the change of Lc values from the equipment reading. For example, TiN coatings on steel substrate display a higher Lc value than that on Ti alloy substrate[6].

Researchers have been spending a lot of effort to determine the failure mechanism behind the scratch testing. Bull[8] concluded that four different major failure modes including through-thickness coating cracking, chipping, buckling/spallation and plastic deformation, would determine coating failure appearance based on hardness ratio of coating over substrate. In cases of hard coating on hard substrate with different interfacial strength, the adhesion-related failures were also summarized as Buckling, Wedge spallation and Recovery spallation. Solutions were also proposed to avoid above failures, such as reducing the size of interfacial defects and increasing the coating toughness.

With the continued exploration on scratch failure modes, it is evident that realistic theoretical models for the scratch process are both important and necessary. Holmberg et al.[9] proposed a model comprising elastic, plastic and fracture behavior of the scratch process by using the three-dimensional finite element method. They suggested the first crack occur due to accumulated tensile stresses exceeding fracture limit of coating from bending and pulling action. The theoretical studies on scratch process also inspire an automatic evaluation approach for adhesion strength by the method of convolutional neural networks[10].

Focused ion beam (FIB) technology can reveal more details[11]. Hoy et al.[14] found that

complete coating removal might be absent even under high applied loads, where there was cracking but no extensive chipping outside of the scratch track. Kleinbichler et al.[15] displayed that film buckling induced by scratch, might be a reasonable way to measure adhesion quantitatively. Kareer et al.[16] presented the residual deformation field map around a nanoscratch track at a constant normal force of 3mN. Those studies on scratch failures proved experimental feasibility to study a typical scratch track. However, such a microscopic study is time consuming and is limited by the equipment capability for imaging cross-sectional scratch under a FIB-SEM. An accurate and yet practical method is desired to study the scratch failure modes.

As a widely studied coating, TiN coatings are used in many industrial applications to date[17] which was adopted in this study to build the model thin film system. In this study, details of the failure modes after a scratch test were studied in details in model system. For the first time, we used this model coating to study the cross-sectional level from a simple but robust way to for sample preparation. We presented the whole scratch length to probe the failures at different stages. This study contributes to the existing contact mechanism in micro-scale, guiding coating design and manufacturing processes.

2. Experimental procedures

2.1 Film Deposition

A multi-arc ion plating system (Hauzer Flexicoat 850, Hauzer Techno Coatings BV, The Netherlands) was used to fabricate TiN films. Detailed description of the coating deposition system is illustrated in reference[18]. Two rows of titanium targets (Φ104.8 mm×8 mm, 99.95% purity, three targets each row) were equipped in the inner side of vacuum chamber as the cathode arc sources. 304L stainless steel coupons (30mm×30mm×2mm) were chosen as substrates, and were mounted on a sample holder with a speed of 3rpm, after being cleaned ultrasonically with acetone and ethanol for 30 minutes respectively.

Prior to deposition, the substrates were ion etch cleaned by Ar ions for 30 minutes with bias voltage of -1200V, Ar gas flow rate of 50sccm and vacuum temperature of 450℃ after the pressure of vacuum chamber was pumped down to less than 5×10^{-3}Pa. A Ti buffer layer was deposited prior on the 304L substrate surface to promote the film adhesion, with bias voltage of -25V, Ar gas flow rate of 300sccm, temperature of 450℃ and each Ti target current of 100A for 10minutes. Subsequently, the TiN film was deposited directly onto the Ti buffer layer with bias voltage of -25V, nitrogen flow rate of 800sccm, temperature of 450℃ and a current of 100A for each Ti target for 180minutes. The bias voltage of -25V during film deposition was adopted in this study aiming to reduce the film residual stress, hence an increased adhesion between film and substrate.

2.2 Mechanical properties characterization

The hardness (*H*) and elastic modulus (*E*) of TiN film was measured using a nano indentation system (TTX-NHT2, Anton Paar) equipped with a Berkovich indenter at room temperature. The nano indentation test was conducted using the load-controlled mode by linear loading, with a loading/unloading rate of 60.0mN/min, and 5s holding time. The maximum indentation load of 30.0mN was selected for the following reasons: a), to guarantee the indentation depth not exceeding 10% of the thickness of TiN film and to eliminate substrate effects[19]; b), to avoid the material loss of indentation tip; c), to ensure the dents were deep enough that the test results were not affected by surface particles of TiN film. The H and E were calculated automatically using the load-displacement

curve according to Oliver-Pharr method. In order to obtain the average H and E, nine indentation tests were completed, with each indent separated from each other by about 30μm.

Adhesion strength of TiN film was evaluated by a scratch tester (RST3, Anton Paar) fitted with a Rockwell "C" diamond stylus (120° cone with a 200μm radius hemispherical tip) at room temperature. Scratch tests were performed using the load-controlled mode by linear loading, with the loading rate of 99N/min, an initial load of 1N and end load of 100N, and scratch length of 5mm. Acoustic emissions (AE) and friction forces were monitored online during scratch testing. The critical loads (Lc1, Lc2 and Lc3) that are used to define the failures of the film can then be determined combining the acoustic emissions curve and microscopy. Six scratches were performed on TiN film samples to obtain the average critical loads.

2.3 Cross-sectional samples preparation and microstructure characterization

The surface morphology and cross-sectional morphology of TiN film scratches were observed by optical microscopy (OM, Axio Lab A1 pol, Carl Zeiss) and scanning electron microscopy (SEM, JSM 6701F, JEOL). The scratched TiN films were glued together with Si wafers to protect the surface of scratch tracks. The cross-sectional sample was then grinded and polished along the cross section direction using sandpaper and diamond suspension until the cross-sectional morphology of the scratch can be found under OM. In this study, the cross-sectional samples in both parallel and perpendicular directions to the scratch direction were prepared, which are defined as cross-section-parallel to scratch direction (CSPara) and cross-section-perpendicular to scratch direction (CSPerp), for the purpose to observing the cross-sectional morphology of scratches more in detail. Two scratches displaying similar scratch test results were selected and then prepared as cross-sectional samples. Besides, various cross-sectional planes were prepared at different scratch locations as shown in Fig. 1(a) and (b) schematically, including CSPara and CSPerp. Please note that T_a-T_c and S_a-S_k mark only approximate locations rather than exact positions of the cross sections.

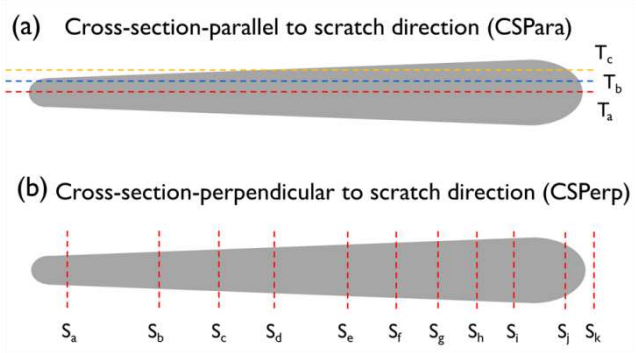

Fig. 1 Schematic view of the cross-sections selected for observing at different locations of scratches of (a) CSPara, and (b) CSPerp

3. Experimental results

3.1 Microstructure, Hardness and Elastic modulus of TiN film

SEM images of planar and cross-sectional morphologies of the TiN film are shown in Fig. 2(a) and (b), respectively. The planar SEM image of TiN film shows a typical arc ion plating morphology, with quantities of droplets existing on the film surface due to the incomplete evaporation of arc target material. According to the cross-sectional SEM image of TiN film, the total film thickness is around

9.5 μm, while the thicknesses of Ti buffer layer and TiN layer are around 600nm and 8.9μm respectively. The side view of the liquid droplets, which look like asperities were observed. Black spots on the cross-section surface of TiN film are stain residue after the polishing process. XRD pattern of the as-deposited TiN film shown in Fig. 2(c) displays the film diffraction peaks of (111), (200), (220), (311) and (222) (JCPDS-ICDD NO. 65-5759), which represents TiN face-centered cubic structure. The sharp diffraction peaks indicate a good crystallinity of TiN film.

The average hardness and elastic modulus of TiN are determined as 27.2 GPa and 318.8 GPa respectively, which are typical for TiN film deposited by arc ion plating[20]. The maximum indentation depth is around 400 nm (which is less than 1/10 of the film thickness), indicating no substrate effects to the H and E test results.

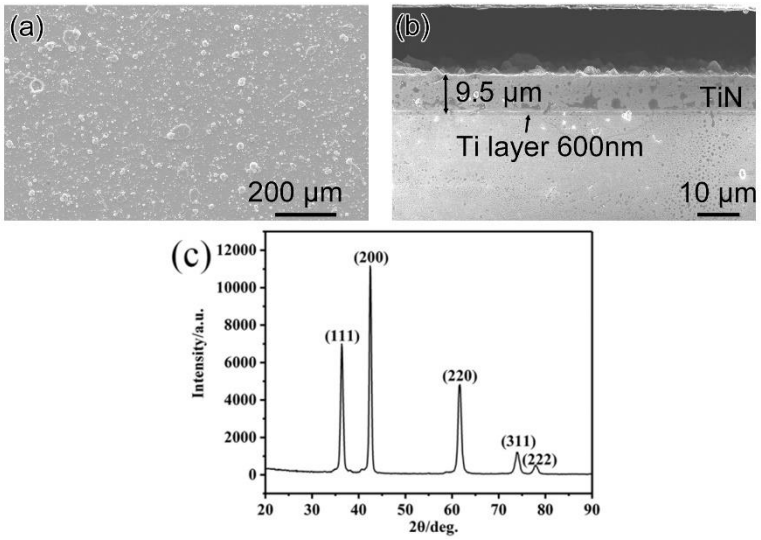

Fig. 2 SEM images of (a) planar and (b) cross-sectional morphologies of TiN film; (c) XRD pattern of TiN film

3.2 Scratch test results of TiN film

Fig. 3(a) and (b) show the superficial and corresponding cross-sectional morphologies of the TiN film scratch track respectively, with identical scales. According to the acoustic emission signal curve in Fig. 3(c) and SEM images of the scratch track in Fig. 3(d), the critical loads of Lc1, Lc2 and Lc3 are determined as 20 N, 40 N, and 65 N respectively. Lc1 indicates the initiation of cracking which is mainly located at the edges of the scratch track. Lc2 is assigned to the first adhesive failure or first chipping point, which mostly displays spalling failure mode. Lc3 is defined as the critical load where the film is completely peeled off the substrate, exposing the substrate completely. Before Lc3, the coating remains mostly intact. Three scratch tests displaying similar results were performed on TiN film samples to obtain the average critical loads in this study. The length of scratch track is 5mm as shown in Fig. 3(b), which represents the cross-sectional morphology of TiN film scratch (marked as cross-section T_a as shown in Fig. 1). The start and end locations of the scratch track are marked out accordingly.

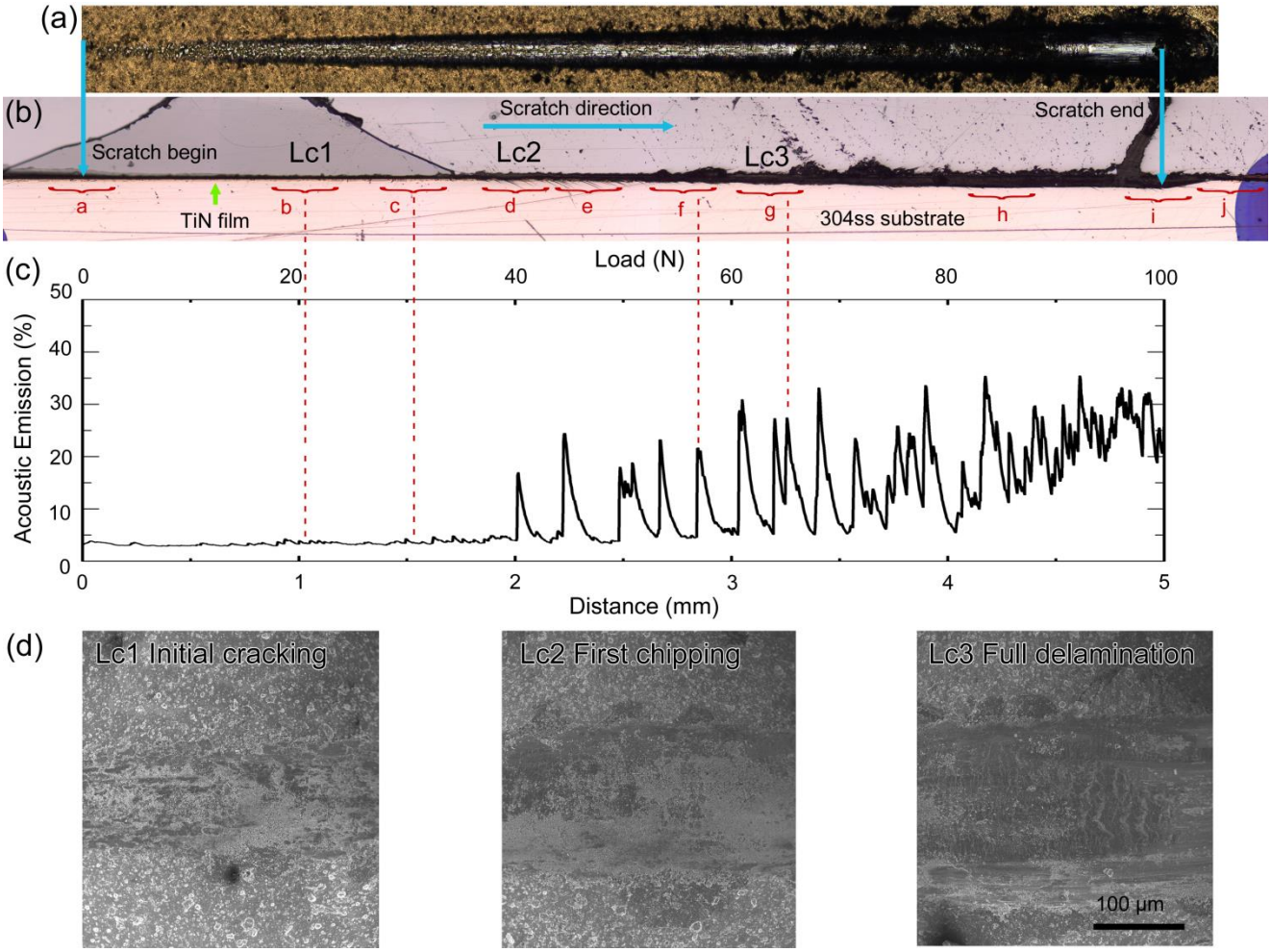

Fig. 3 Scratch test data of TiN film, (a) OM superficial image of scratch track, (b) Morphology of CSPara of TiN film, marked as cross-section T_a as shown in Fig. 1, (c) Acoustic emission signal as a function of scratch distance, (d) SEM images of the critical loads locations, SEM images with same scale bars

3.3 Cross-sectional morphology of scratch of TiN film parallel to scratch direction

Fig. 4(a)-(j) (belong to position T_a in Fig. 1) shows the magnified OM cross-sectional morphologies in locations a to j in Fig. 3(b) in order to analyze the scratch track more clearly. Fig. 4(a) shows that no cracks are generated at the start of the scratch track. Lc1 is determined as 20N since the first obvious crack can be seen in Fig. 4(b), corresponding to location b. The cracks in Fig. 4(b) and (c) are recognized as cohesive failure rather than adhesive failure[4], as they are not through film cracks. The crack propagation is hindered due to the lower stresses in such scratch loads being unable to propagate cracks thoroughly. In the meantime, the crack propagation process will release the generated stress. The cohesive failure is not an adhesion-related failure mode generally, so Lc1 cannot be determined as the adhesion-related critical load in this paper. Meanwhile, it can be found that the cohesion-related cracks in locations b and c produce little amounts of acoustic emission signals as shown in Fig. 3. Through-film cracks and film delamination is seen in Fig. 4(d), corresponding to location d in Fig. 3, with sharp acoustic emissions at 40N. As the stylus moves forward, the gradually accumulated stress peeled the film off and destroyed the integrity of the film, leading to such crushing-like morphology.

Fig. 4(e)-(g) are the magnified images of locations e to g in Fig. 3 respectively. As the load increases, TiN film exfoliates more seriously at these phases, from partial delamination to totally peeling off after the location g. Thus, Lc3 is determined to be around 65N. The images display wave-like morphology for both the 304L substrate and the TiN film. In Fig. 3(c), the corresponding AE signal also acts in pulse mode, which an AE signal peak is followed by the gradually decreased AE signal. Increasing the load, the accumulated stress applied on the coating/substrate system increases, causing the breakage of the TiN film, the substrate deformation, and furthermore the stress relief phenomenon. The repeated process, which is '(1) stress accumulating- (2) coating peeling off and failure- (3) stress relief', induced the wave-like morphology and the AE signal pulse mode. Due to the intense stress in front of the stylus, the film crushes into small loose particles from a whole block.

Fig. 4(h) displays a smooth and film-free surface which is caused by the TiN film fully peeling off the substrate. The wave-like morphology also disappears, which is a significant indication that 304L substrate yields completely due to the accumulated stress in front of the stylus. Fig. 4(i) and (j) shows the images of the scratch end located in i and j positions in Fig. 3 respectively. The film peels off completely and followed by a significant substrate deformation that induces a bulge of the substrate in front of the stylus. It also shows that the TiN film pieces are pressed into the substrate.

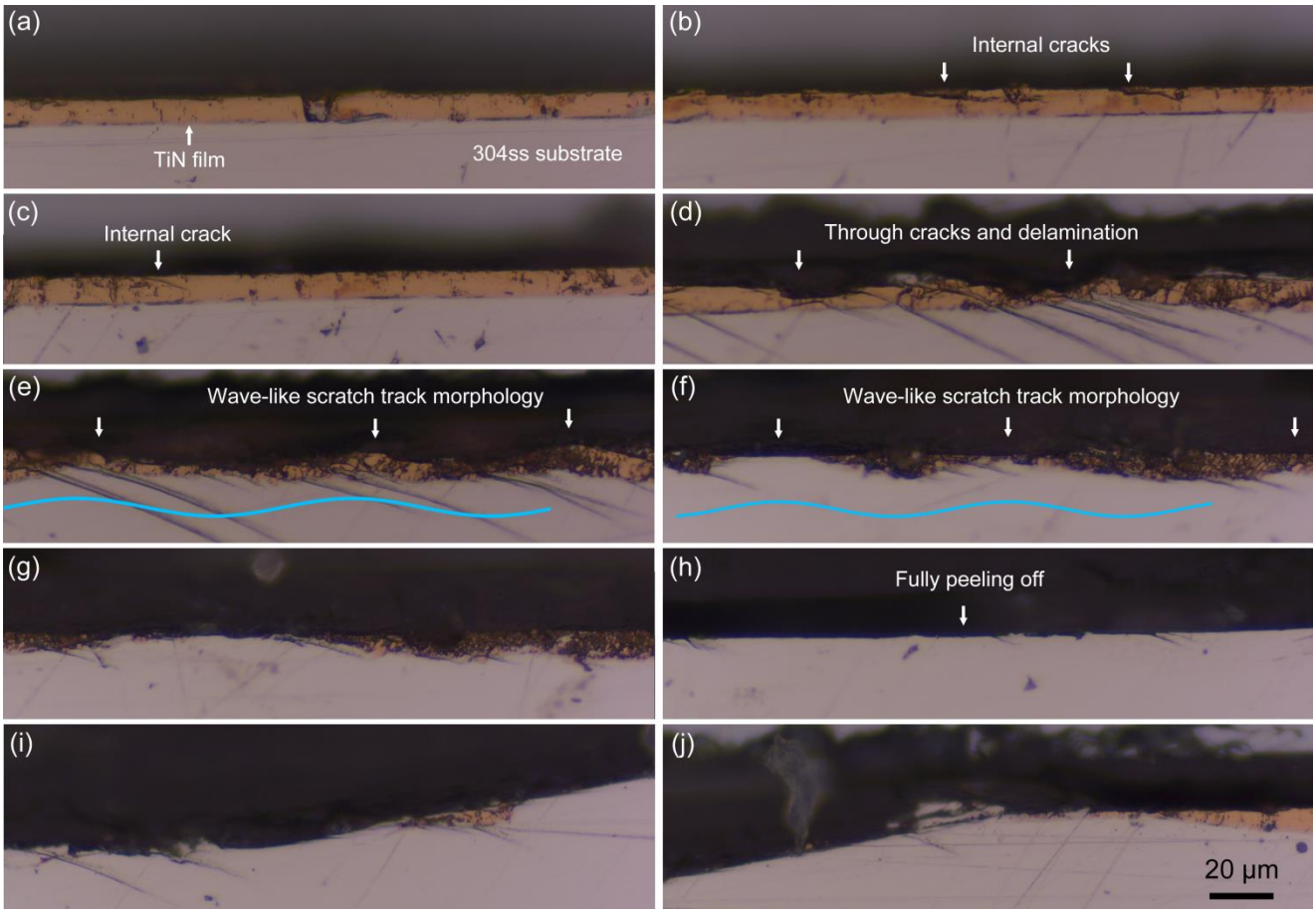

Fig. 4 (a)-(j) magnified OM images in locations a-j in Fig. 3, scale bar applied to all images

The cross-sectional OM images of cross section T_b are shown in Fig. 5. Cross section T_b is at a distance from T_a. Since the stylus has a spherical shape, the scratch depth of T_b is lower than that of T_a. Although the failure in T_b is not as severe as that in T_a, coating delamination and material loss are

still visible. Fig. 5(b) and (c) show that no cracks are generated before location c. Crack and delamination can be seen in Fig 5(d), from which the partial delamination of the TiN film can be ascribed to the spallation failure mode[3]. It should be noticed that the delamination occurs inside the film but not in the film/substrate interface, so this is a cohesive failure rather than an adhesive failure. Fig. 5(e) shows the peeling off and through-thickness cracks of the film. It is shown in Figs. 5(f)-(j) that the TiN pieces are pressed into the substrate. These TiN pieces, mainly with blade shape, are probably coming from the peeled TiN pieces and the residue after delamination. At the end of the scratch track as shown in Fig. 5(k), the substrate and the film deform bulging upwards together in front of the stylus.

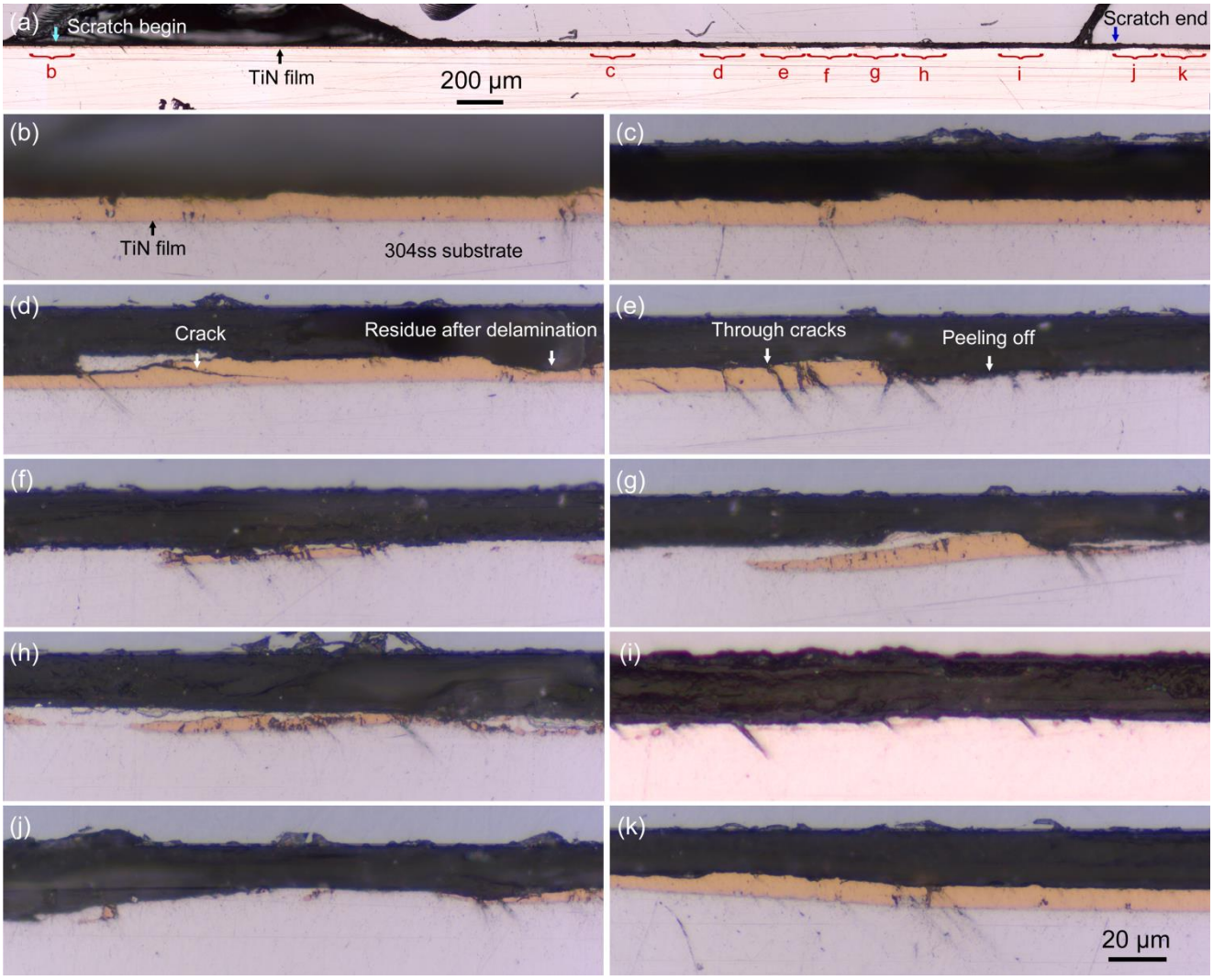

Fig. 5 (a) Morphology of CSPara T_b, (b)-(k) magnified OM images in locations b-k in (a), scale bar in (k) applied to (b)-(k)

The cross-sectional OM images of cross section T_c are shown in Supplementary Fig. S1. Cross section T_c is near the outside of scratch. Only few film failures such as cracks and delamination can be seen. The structural integrity of the film/substrate system is mostly preserved. Before the location d, the film remains undamaged. As shown in Fig. S1(e) and (f), at location e and f, interior cracks and delamination can be seen. Fig. S1(h) and (i) display cracks, delamination and film/substrate deformation at the end of scratch.

3.4 Cross-sectional morphology of scratch of TiN film perpendicular to scratch direction

The cross sections along the perpendicular direction of scratch track are also observed. The SEM morphology of cross-section S_a, which is near the scratch starting position as marked in Fig. 1(b), is shown in Fig. 6. It displays that TiN film deforms together with the 304L substrate. The indentation depth is around 4 μm (measured in Fig. 6) while the Hertz contact stress is estimated as high as 10.5 GPa by using Hertz contact theory. Nevertheless, no obvious cracks were observed at this stage.

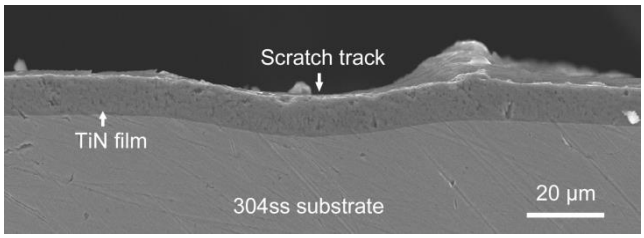

Fig. 6 Morphology of CSPerp S_a

The SEM morphology of cross-section S_b is shown in Fig. 7. Cracks as indicated by the arrows can be seen at the edge of the scratch track in Fig. 7(b) and (d). There are no through thickness cracks, and the cracks are restrained inside the film. No obvious crack can be seen in location c as shown in Fig. 7(c). A slight upward bulge of the substrate and the film can be seen in Fig. 7(d).

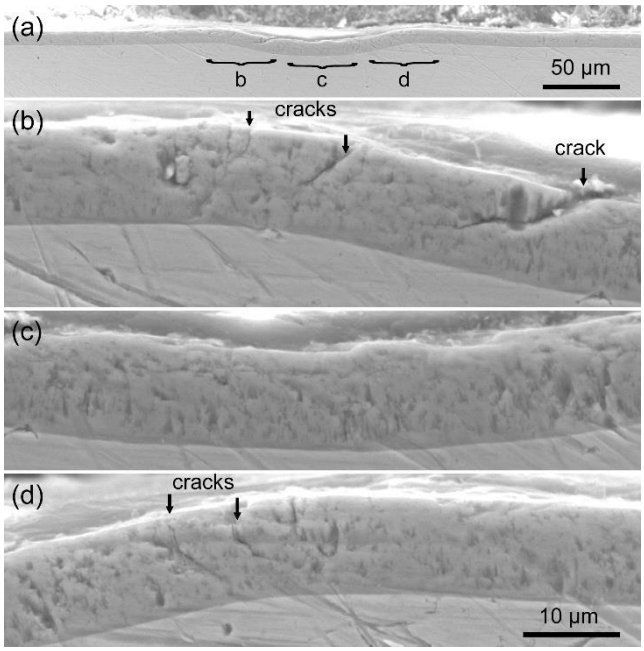

Fig. 7 (a) Morphology of CSPerp S_b, (b)-(d) magnified OM images in locations b-d, scale bar in (d) applied to (b)-(d)

The SEM morphology of cross-section S_c is shown in Supplementary Fig. S2. More and more cracks and failures can be seen at the edge of the scratch track due to the material deformation as indicated by arrows in Fig. S2(b) and (d). But they are still not through thickness cracks. The SEM morphology of cross-section S_d is shown in Fig. 8. Not only cracks but also delamination can be seen

at the edge of scratch track as shown in Fig. 8(a). Quantities of through thickness cracks can be seen along the scratch track as indicated by arrows in Fig. 8(b). The delamination and through thickness cracks illustrate relatively severe film failure. It also shows that the substrate elastic recovery occurs below the delamination zone, which might be attributed to the stress relaxation of film/substrate system during cracking and delaminating.

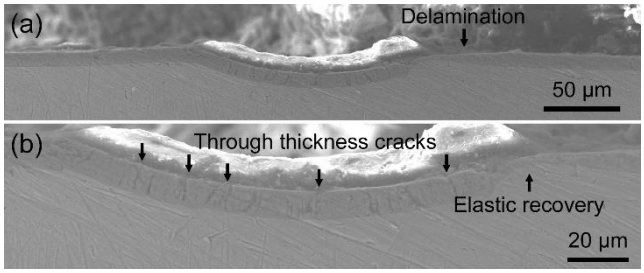

Fig. 8 (a) Morphology of CSPerp S_d, (b) magnified OM image of (a)

The SEM morphology of cross-section S_e is shown in Fig. 9. Through thickness cracks, delamination, and film shear fracture illustrate more and more serious failure of the film. But there is only partial delamination in the scratch track. The shear cracks inside the film and the elastic recovery of the substrate can be found in Fig. 9(b) and (c), which might be the main culprit in the subsequent shear fracture failure. In comparison with Fig. 9(d), the film shear fracture in Fig. 9(b) is therefore deemed the edge spallation in Fig. 9(d).

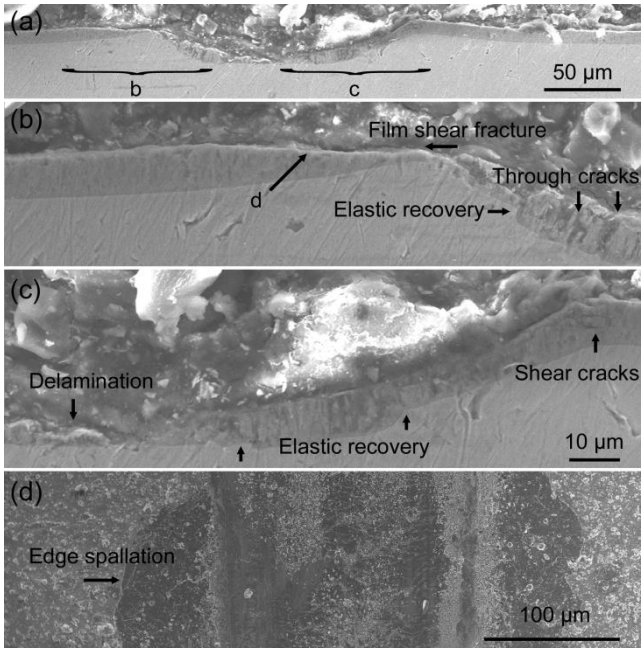

Fig. 9 (a) Morphology of CSPerp S_e, (b)-(c) magnified OM images in locations b-c, scale bar in (c) applied to (b)-(c), (d) surficial SEM image of scratch track showing the edge spallation failure mode

The SEM morphology of cross-section S_f is shown in Supplementary Fig. S3. The film is fully peeled off the substrate in the scratch track. Shear fracture, and the corresponding edge spallation failure mode can be seen in Fig. S3(b)-(d). The SEM morphology of cross-section S_g is shown in Fig.

10. It shows that the film is fully peeled off the substrate. The material residues after scratch at the edge of scratch can be seen in Fig. 10(b)-(c), and their embedded images display the accumulation of material, which resembles the 'built-up edge' during machining. It also shows that the TiN film residues still adhere to the substrate. The corresponding surficial SEM image in Fig. 10(d) confirms the smooth morphology inside the scratch track and the accumulation of material at the edge of scratch track.

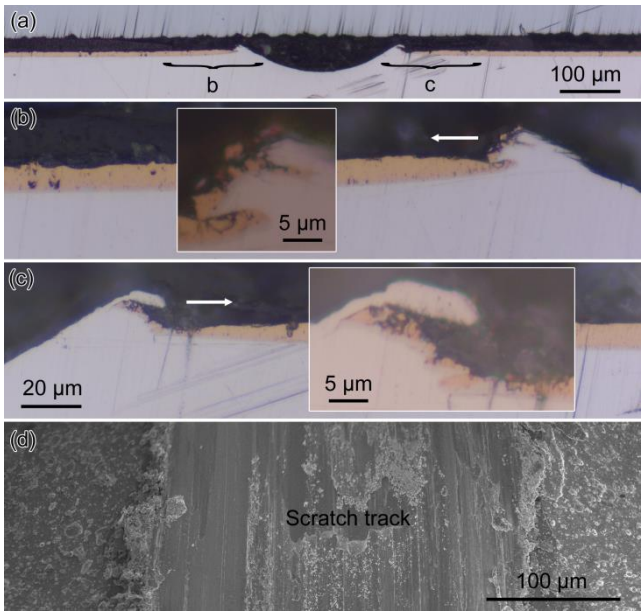

Fig. 10 (a) Morphology of CSPerp S_g, (b)-(c) magnified OM images in locations b-c, cale bar in (c) applied to (b)-(c), (d) corresponding surficial SEM image of scratch track

The SEM morphology of cross-section S_h and S_i is shown in Supplementary Figs. S4 and S5 respectively. The fully peeling off film and the 'built-up edge' morphology can be seen. In Fig. S4, as shown in the inserted magnified image of the area where the white arrow points, a small TiN particle is pressed and wrapped in the scratch track. In Supplementary Fig. S5(b), it can be seen that the bent-shaped TiN film still sticks to the 304L, with some TiN particles being sealed in the steel 'built-up edge'.

The SEM morphology of cross-section S_j is shown in Fig. 11. Even if S_j is located in the front of the stylus, the film is still fully peeled off due to the accumulated stress as shown in Fig. 11(c). In Fig. 11(b), the shear crack can be clearly seen in the TiN film, and a subsequent delamination (as shown in Fig. 11(d)) can be anticipated. The corresponding surficial SEM image in Fig. 11(e) confirms an edge spallation morphology at the scratch end. The SEM morphology of cross-section S_k is shown in Supplementary Fig. S6. S_k is located in front of the stylus and outside the scratch track. The upward bulge and the material deformation are ascribed to the accumulated stress in front of the stylus. It is seen that the TiN film deformed with the substrate simultaneously. Supplementary Fig. S6 indicates the pre-existence of buckle or folding ahead of the stylus, as in references[9].

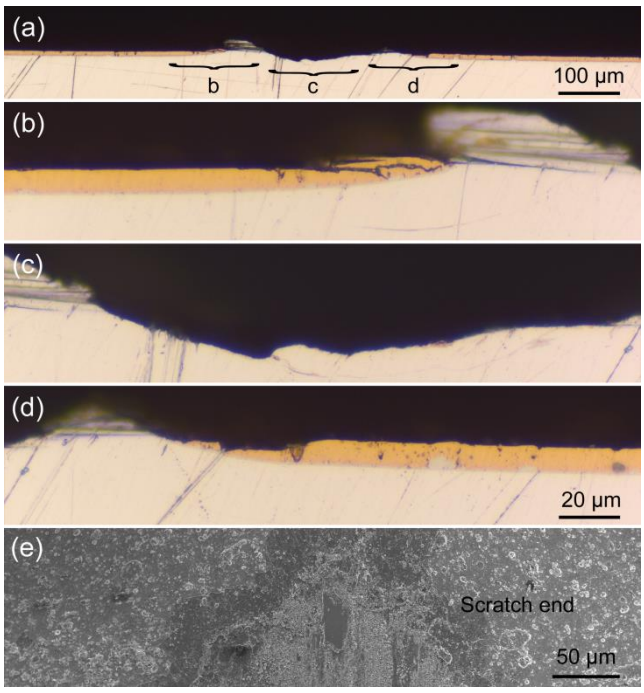

Fig. 11 (a) Morphology of CSPerp S_j, (b)-(d) magnified OM images in locations b-d, scale bar in (d) applied to (b)-(d), (e) corresponding surficial SEM image of scratch track

4 Discussion

4.1 Critical load determination

Generally, Lcs represent different failure modes, such as first scratch crack (Lc1), first delamination (Lc2), and film peeling off (Lc3). Our results showed the model TiN thin film system is capable to capture the full scenarios from Lc1 to Lc3 as was report in many TiN common literature[5]-[7]. Fig. 3 also display that the first AE peak cannot be arbitrarily determined as Lc1. From the SEM image in Fig. 3, Lc1 is around 20N. Meanwhile, Lc2 is determined as 40N, which is similar with that in the literature[6]. It corresponds to the first AE peak, and marks the first delamination outside the scratch track. But this delamination resembles a cohesive failure rather than an adhesive failure as shown in Figs. 8 and 9. Besides, there is no clear evidence that Lc2 corresponds with the first AE peak according to its definition[1]. Lc3 is determined as 65N from OM images and cannot be corresponded to any of the AE characteristic peaks. From above, it is concluded that the AE signal alone is insufficient to determine the film critical loads for this hard film/soft substrate system[5].

4.2 Cohesive, adhesive failure, and evolution of edge spallation

According to the location and propagation depth of the cracks, the failure modes during scratch test for the hard film/soft substrate system can be expressed as three main categories[4]: (1) cohesive failure in coating, (2) cohesive failure in substrate, and (3) adhesive failure as shown in Fig. 12. Lc1 corresponds to cohesive failure in the film as shown in Fig. 12(a), where the first crack emerges but is still restrained in film due to the relatively low stress. In Fig. 12(b), instead of peeling off along the film/substrate interface, the cracks propagate into the substrate as a response when the film adhesion strength is overwhelmingly strong. Lc2 has long been recognized as adhesive failure, and features mostly a fish scale like edge spallation. However, the results in this paper indicate that the edge

spallation can be the cohesive failure rather than adhesive peeling as shown in Fig. 9 and Fig. S3, where the cohesive delamination occurs. It is therefore debatable whether and when Lc2 can be deemed as adhesive failure.

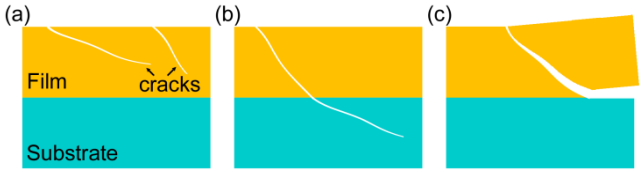

Fig. 12 Failure modes of film (a) cohesive failure in film, (b) cohesive failure in substrate, (c) adhesive failure

The process on how the edge spallation occurs is suggested as the following steps: i) As shown in Fig. 13(a), when the stylus is applied with load and scratch forwards, the film and substrate deform simultaneously. Crack is generated at the scratch edge where the most serious stress concentration area locates, while the edge stress is higher than the film fracture strength. At this stage, the film/substrate system deformation is mild, and the crack expands into film at a certain angle with film surface. Figs. 7 and S3 show the corresponding SEM images. ii) As the load increases, the film/substrate system deformation becomes intense, inducing the bulge-like morphology as shown in Fig. 13(b). Due to the film/substrate system is jacked up by the bulge, the crack propagates parallel to the film surface, which is similar to Fig. 11(b). iii) In Fig. 13(c), as the load increases further, the edge spallation would occur when the stylus continues to scratch forward, as can be seen in Figs. 8-9 and Fig. S3. Therefore, even if the first edge spallation or chipping are defined as Lc2, they cannot be considered as the adhesive failure in this study, since it is not an interfacial crack between the film and substrate. In other words, using Lc2 as the criteria to evaluate film adhesion strength is illogical. The effect of material deformation (E.g. bulge) on the fracture and crack deflection should be also concerned in this case. The edge spallation failure is thus shear induced cohesive failure in film rather than the adhesive failure as is usually deemed. The evolution and stress status of the main crack which induced the edge spallation should be concerned significantly and might be one key to understand the fracture mechanism.

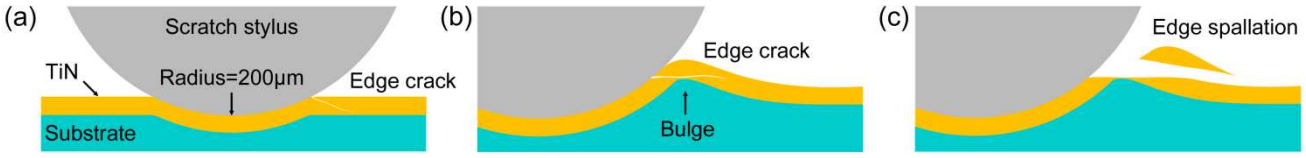

Fig. 13 Process of edge spallation failure (a) crack generation at the edge of scratch track, (b) crack propagation and material deformation, (c) shear fracture. In all figures the scratch orientation is into the page.

4.3 Three stages of the whole scratch evolution

Stage 1: TiN film remains adhering onto substrate

As the above results show, at the initial loading of the scratch test, TiN film will remain adhering onto the 304L substrate due to the mild stress field generated by low loading force. The scratch groove is also not deep in depth. The corresponding material response at this stage could be explained as in ref.[9], in which Holmberg et al. proposed three independent phases to interpret the material response when the stylus was drawn along a hard coating, which are *ploughing, interface*

sliding, and coating pulling. The fracture of TiN induced by *coating pulling* can be seen in Fig. 4, where small amount of cracks were generated by scratch stylus pulling one-side-fixed TiN film under friction force. The low density cracks are mainly internal cracks inside the TiN film in this stage (shown in Fig. 4) due to the mild stress field. Although *ploughing wear* and *plastic deformation* would occur, they are subdominant material responses at this stage. Other than the mild stress field, the high hardness, and large thickness of TiN film are possibly the other two main reasons for this. It is clear at stage 1 that TiN film remains integral and would protect the substrate effectively even with cracks emerging. The TiN/304L stainless steel (TiN/304L) system is used in this study, which is deemed as a 'hard film/soft substrate' system. It should be noticed that the overall deformation of this system could be bigger than that of a 'hard film/hard substrate' system, in terms that the 304L hardness is significant lower than TiN film. As a result, the process of stage 1 is relatively short in comparison with a 'hard film/hard substrate' system. Meanwhile, it could be speculated that the process of stage 1 should be longer for a 'hard film/hard substrate' system regarding its better load bearing capacity by the hard substrate, which is considered to be one of the reasons that harder substrate will endow film higher adhesion properties[4].

Step 2: TiN film break thoroughly due to high stress and strain

Step 2 describes the material response when TiN film breaks thoroughly and more severe failures occur. Stress field condition would become more and more severe as the loading force increased gradually, and would follow by the large plastic deformation. The plastic deformation of 304L would be dominant in the overall plastic deformation of TiN/304L system, because the yield strength of 304L is much lower than that of TiN. Meanwhile, TiN film would generate brittle fractures when overwhelming stress was applied, and its fracture strength was surpassed on the premise that TiN film material should be brittle. Severe fracture and thorough cracks would occur inside the TiN film and result in huge amounts of TiN particles. Hence, the chipped TiN layer would have no effective protection on the substrate at stage 2, where the scratch stylus would press into substrate, and severe ploughing wear inside the 304L substrate is predicted.

Step3: ploughing wear into steel materials and pile up in front of stylus

Before the ploughing wear into the substrate occurring, the TiN hard film possesses the ability of preventing the substrate from ploughing. Although it is known that TiN film and other hard films generally have high friction in dry air conditions, the scratch tests results show that they would still feature anti-ploughing property. And thus the TiN film would remain its integrity on the scratch track surface to prevent the ploughing wear of the substrate, which is one advantage of producing the hard films on the metal soft substrates.

When the loading force increases continuously, the stylus would penetrate into 304L substrate more easily without the protection of fragmented TiN. Material pile-up in front of the stylus and severe ploughing wear inside the 304L substrate would occur, thus lifting up the TiN film in front of the stylus and peeling it off. TiN film would give negligible protectiveness at this substrate large plastic deformation circumstance. The film pieces could be pressed into the substrate by the passing indenter at this stage as shown in Supplementary Fig. S4.

Lc1, Lc2, and Lc3 are well defined from an engineering perspective, and they are widely used to quantify the adhesive failures of film/substrate system. Lc1 indicates the initiation of cracking which mainly located at the edges of the scratch track. Lc2 is assigned to the first adhesive failure or first chipping point, which displays spalling failure mode mostly. Lc3 is defined as the critical load that the film is completely peeled off the substrate, while the substrate is exposed completely[1]. However,

for the TiN/304L system in this study, the spallation failure at the edge of track is actually cohesive failure in film (shown in Fig. 13), not an adhesive failure (Lc2).The Lc3 position corresponds to cohesive failure in substrate rather than film peeling off completely. Thus, it is concluded that the critical loads would not correspond to adhesive failures in this TiN/304L system. Although Lc1, Lc2, and Lc3 can be easily obtained in this TiN/304L system, they could not be deemed as adhesive failures explicitly. Moreover, significant differences might appear for the films between the Lc measurement results and their actual use. Thus, more care should be paid in terms of using Lc to interpret the adhesion properties of other film/substrate systems, and the adhesion of film should be evaluated by considering the whole film/substrate system, not solely superficial analysis of the film surface.

5 Conclusion

A model TiN thin film system were deposited on 304L stainless steel substrate by multi-arc ion plating method. The cross-sectional and surficial morphologies of scratch tracks on such a system were investigated in terms of the material response and failure modes during a scratch process. The methodology is transferable to study other model thin film system. The conclusions are summarized as:

(i) A series of microscopic deformation, fracture and tribology mechanisms, including cracks, substrate plastic deformation, synergistic bulge deformation at the scratch track edge, pile-up in front of the stylus, fragmentation of TiN film, and ploughing wear, were all visualized for the first time in the whole scratch.

(ii) The cross-sectional morphology of the edge spallation reveals a cohesive failure inside the TiN film at Lc2 position, which was commonly known as adhesive failure definition of Lc2. The Lc3 position corresponds to cohesive failure in substrate, rather than the film completely peeling off the substrate.

(iii) Determine the adhesion levels using Lc values should take a greater care by evaluating the whole film/substrate system. This study may provide a transferable methodology in thin film failure analyses when in depth details are required.

Acknowledgements

This work is supported by the National Natural Science Foundation of China [grant number 51405476]; and the Natural Science Foundation of Gansu Province [grant number 18JR3RA382]. The authors are grateful for facility access support by the Engineering and Physical Sciences Research Council (EPSRC, Grant no. EP/R02524X/1) in the UK.

References

[1] N.X. Randall, The current state-of-the-art in scratch testing of coated systems, Surf. Coat. Technol. 380 (2019) 125092.

[2] Z. Chen, K. Zhou, X. Lu, Y. Lam, A review on the mechanical methods for evaluating coating adhesion, Acta Mech. 225 (2014) 431-452.

[3] S.J. Bull, E.G. Berasetegui, An overview of the potential of quantitative coating adhesion measurement by scratch testing, Tribol. Int. 39 (2006) 99-114.

[4] A.J. Perry, Scratch adhesion testing of hard coatings, Thin Solid Films. 107 (1983) 167-180.

[5] M. Bromark, M. Larsson, P. Hedenqvist, M. Olsson, S. Hogmark, Influence of substrate

topography on the critical normal force in scratch adhesion testing of TiN-coated steels, Surf. Coat. Technol. 52 (1992) 195-203.
[6] J. Stallard, S. Poulat, D.G. Teer, The study of the adhesion of a TiN coating on steel and titanium alloy substrates using a multi-mode scratch tester, Tribol. Int. 39 (2006) 159-166.
[7] A. Rodrigo, P. Perillo, H. Ichimura, On the correlation of substrate microhardness with the critical load of scratch adherence for hard coatings, Surf. Coat. Technol. 124 (2000) 87-92.
[8] S.J. Bull, Failure mode maps in the thin film scratch adhesion test, Tribol. Int. 30 (7) (1997) 491-498.
[9] K. Holmberg, A. Laukkanen, H. Ronkainen, K. Wallin, Tribological ananlysis of fracture conditions in thin surface coatings by 3D FEM modeling and stress simulations, Tribol. Int. 38 (2005) 1035-1049.
[10] B. Lenz, H. Hasselbruch, H. Grobmann, A. Mehner, Application of CNN networks for an automatic determination of critical loads in scratch tests on a-C:H:W coatings, Surf. Coat. Technol. 393 (2020) 125764.
[11] T. Vodenitcharova, O. Borrero-Lopez, M. Hoffman, Mechanics prediction of the fracture pattern on scratching wafers of single crystal silicon, Acta Mater. 60 (2012) 4448-4460.
[12] M. Kabir, P. Munroe, Z.F. Zhou, Z.H. Xie, Scratch adhesion and tribological behavior of graded Cr/CrN/CrTiN coatings synthesized by closed-field unbalanced magnetron sputtering, Wear. 380-381 (2017) 163-175.
[13] Y.Q. Wang, R. Fritz, D. Kiener, J.Y. Zhang, G. Liu, O. Kolednik, R. Pippan, J. Sun, Fracture behavior and deformation mechanisms in nanolaminated crystalline/amorphous micro-cantilevers, Acta Mater. 180 (2019) 73-83.
[14] R. Hoy, V.G.M. Sivel, J.D. Kamminga, G.C.A.M. Janssen, Failure during scratch testing of thick and thin CrN coatings examined using focused ion beam, Surf. Coat. Technol. 200 (2005) 149-152.
[15] A. Kleinbichler, M.J. Pfeifenberger, J. Zechner, S. Wohlert, M.J. Cordill, Scratch induced thin film buckling for quantitative adhesion measurements, Mater. Des. 155 (2018) 203-211.
[16] A. Kareer, E. Tarleton, C. Hardie, S.V. Hainsworth, A.J. Wilkinson, Scratching the surface: Elastic rotations beneath nanoscratch and nanoindentation tests, Acta Mater. 200 (2020) 116-126.
[17] Q.C. Chen, A. Li, G.Z. Wu, Z.B. Lu, G.A. Zhang, G.K. Tian, Structure vs chemistry: Tribological behavior of TiN films in the nitrogen atmosphere, Ceram. Int. 46 (2020) 28053-28063.
[18] Q.C. Chen, G.Z. Wu, D.S. Li, A. Li, L.L. Shang, Z.B. Lu, G.A. Zhang, Z.G. Wu, G.K. Tian. Understanding the unusual friction behavior of TiN films in vacuum, Tribol. Int. 137 (2019) 379-386.
[19] R. Saha, W.D. Nix, Effects of the substrate on the determination of thin film mechanical properties by nanoindentation, Acta Mater. 50 (2002) 23-38.
[20] C.L. Zhao, Y.B. Zhu, Z. Yuan, J. Li, Structure and tribocorrosion behavior of Ti/TiN multilayer coatings in simulated body fluid by arc ion plating, Surf. Coat. Technol. 403 (2020) 126399.
[21] E. Vancoille, J.P. Celis, J.R. Roos, Mechanical properties of heat treated and worn PVD TiN, (Ti, Al)N, (Ti, Nb)N and Ti(C, N) coatings as measured by nanoindentation, Thin Solid Films. 224 (1993) 168-176.